

Role of Temperature in Na₂SO₄–K₂SO₄ Deposit Induced Type II Hot Corrosion of NiAl Coating on a Commercial Ni-Based Superalloy

Yaping Wang,* Rishi Pillai, Elena Yazhenskikh, Martin Frommherz, Michael Müller, and Dmitry Naumenko

The life span of gas turbine coatings may be restricted by type II hot corrosion when exposed at elevated temperatures in aggressive environments during service. Herein, the temperature dependence of corrosion morphologies and kinetics of NiAl coating on a second-generation single crystalline Ni-based superalloy is studied to provide an insight into the possible corrosion mechanisms. A series of tests are performed at 600-800 °C in air-300 ppm SO₂ atmosphere with Na₂SO₄-20% K₂SO₄ salt mixture as deposit. Severe attack is observed at both 700 and 750 °C after 24 h exposure, whereas at 600 and 800 °C, only a minor attack is found. The results indicate that the corrosion rate is strongly governed by Na₂SO₄-NiSO₄ liquid formation, and temperature affects the attack rate of the outer coating (mainly β-NiAl phase) primarily by changing the required minimum SO₃ partial pressure to stabilize this liquid. The influence of temperature and p_{SO_2} on phase equilibrium of the salt and oxide mixture is calculated with an in-house developed thermodynamic database. The predicted minimum p_{SO_3} for liquid formation calculated with the database is consistent with the experimental results.

1. Introduction

Uncoated and coated (overlay or aluminized) structural Ni-based superalloys are widely used in gas turbine and jet engine components due to their excellent mechanical properties and oxidation resistance. These materials undergo accelerated oxidation during service at 600–1000 °C in aggressive sulfur-containing

Y. Wang, Dr. R. Pillai, Dr. E. Yazhenskikh, Dr. M. Müller, Dr. D. Naumenko Institute of Energy and Climate Research (IEK-2)

Forschungszentrum Juelich

Wilhelm-Johnen-Straße, Juelich 52428, Germany

E-mail: ya.wang@fz-juelich.de

Dr. M. Frommherz

Schadensanalyse, Tribologie und Korrosion (TEWS)

MTU Aero Engines, AG

Dachauer Strasse 665, München 80995, Germany

The ORCID identification number(s) for the author(s) of this article can be found under https://doi.org/10.1002/adem.201901244.

© 2020 The Authors. Published by WILEY-VCH Verlag GmbH & Co. KGaA, Weinheim. This is an open access article under the terms of the Creative Commons Attribution License, which permits use, distribution and reproduction in any medium, provided the original work is properly cited.

DOI: 10.1002/adem.201901244

atmospheres in the presence of alkali and alkaline sulfate-containing deposits.^[1] Such rapid degradation induced by sulfate deposit is defined as hot corrosion, his which has been extensively investigated by numerous researchers in the past decades. Depending on the exposure temperatures and the melting point of the deposit, hot corrosion can be further categorized as high-temperature hot corrosion (type I) and low-temperature hot corrosion (type II). Compared with type I hot corrosion, type II is less extensively investigated and the corresponding mechanisms remain unclear.

Most of the conventional hot corrosion investigations were performed using Na_2SO_4 as the deposit.^[4-6] However, in practice, other sulfates, e.g., MgSO₄, CaSO₄, and K₂SO₄, are frequently identified on the surface of turbine components.^[1] Their presence might play a

positive or negative role in the hot corrosion attack. In this regard, K_2SO_4 is usually categorized as aggressive due to its similar chemical properties as those of Na_2SO_4 . According to the work on hot corrosion of iron–aluminum alloys by Shi et al.^[7] the addition of K_2SO_4 into Na_2SO_4 deposit did not change the corrosion mechanism, but shortened the incubation period and accelerated the following attack, due to the formation of lower melting temperature sulfate mixtures.

In most of Na₂SO₄-induced hot corrosion studies, the accelerated attack was only observed in the presence of molten salt. It is thereby generally agreed that liquid formation is a prerequisite for the occurrence of severe low-temperature (type II) hot corrosion. For Na2SO4-induced hot corrosion of Ni- and Co-based superalloys, the major mechanism of the attack is the Na₂SO₄–NiSO₄/CoSO₄ liquid formation, which results from the reaction between Na₂SO₄, NiO/Co₂O₃, and SO₃, and therefore is a function of p_{SO_3} and temperature. Luthra^[4,8,9] estimated the minimum p_{SO₃} required for CoSO₄-Na₂SO₄ and NiSO₄-Na₂SO₄ liquid formation based on the phase diagrams of binary sulfates. In Luthra's work, the activity of CoSO4 in the liquid solution was estimated based on the assumption that the melt consisted of molecular species, which does not agree with the ionic Ni/Na sulfates liquid solution in reality. Misra et al. $^{[10,11]}$ optimized the liquid solution mode by introducing a random

www.aem-journal.com



distribution of cations and calculated the minimum p_{SO_3} required for the liquid formation in NiSO₄–Na₂SO₄ system. However, in Misra's work, the effect of components' composition and temperature on the interaction energy parameter ω_L , which is important for Gibbs energy calculation, was not considered. The ω_L was assumed to be constant and was determined based on the measurements of NiSO₄ content in the molten salt, which could introduce potential experimental errors. Nevertheless, this dilute solution approximation is not reliable at lower temperatures, due to much higher content of NiSO₄ in the salt.

Although hot corrosion rate of Ni-based superalloys and coatings is mainly governed by the NiSO₄-Na₂SO₄ liquid solution formation in the early stage, it is also affected by the presence of other alloying elements which could subsequently oxidize, dissolve into the molten salts, and sulfidize. Various alloying elements are generally known to be present in the aluminide coatings due to interdiffusion processes during the coating manufacturing (aluminizing).[12,13] Some important elements for type II hot corrosion investigations are Al, Cr, Co, W, Mo, etc. [4,6,14–16] They are oxidized or sulfidized during exposure to oxygen- and sulfur-containing environments. First of all, the formation of sulfides consumes sulfur, alters the p_{SO_2} at the oxide/salt interface, and thereby affect the NiSO₄–Na₂SO₄ liquid formation process.^[17,18] Moreover, these alloying elements oxidize and dissolve into the deposit by reacting with Na2SO4, change the SO_3 content of the salt, and therefore, change the acidity of the salt. [4,6,14–16] The dissolution of oxides into the salt can be categorized as two types according to the acidity of the salt. Considering the dissolution of Al₂O₃ into Na₂SO₄ as an example, if the salt is acidic, Al₂(SO₄)₃ will be produced, and the relevant dissolution is called acidic fluxing. Conversely, if the salt is basic for Al₂O₃ dissolution, NaAlO₂ will form, and the dissolution is therefore called basic fluxing.^[2]

The complexity of the problem limits the hot corrosion research mainly to a phenomenological testing of different alloys.^[1,2] Research directed toward a theoretical understanding of the reaction mechanisms to identify the factors governing the corrosion rates and to develop predictive methods for evaluation of hot corrosion is essential. As the reactions are complex, it is

time consuming to experimentally vary all the main parameters, especially p_{SO_3} and temperature. Thermodynamic calculation is therefore an essential method to assist the study. In many hot corrosion studies, the stability diagrams from Luthra^[4,8,9] and Misra et al.^[8,11] are used to predict the conditions for the occurrence of hot corrosion. However, due to the reasons discussed earlier, it is necessary to further verify the NiO–SO₃–Na₂SO₄ stability diagram using newly assessed thermodynamic data.

In this work, we will report type II hot corrosion behavior of NiAl coating on a second-generation Ni-based superalloy at various exposure temperatures with a salt mixture of Na₂SO₄–20% K₂SO₄. Different to previous studies with high SO₂ contents, $^{[19-21]}$ air-300 ppm SO₂ was used in this work to find out the critical conditions of liquid stabilization and subsequent initiation of hot corrosion. In addition to experiments, the stability diagram of Na₂SO₄–NiO–SO₃ and the phase equilibria as a function of temperature and $p_{\rm SO_3}$ were calculated and compared with the literature data, thereby reassessing the calculations in the studies by Misra et al. $^{[8,11]}$ Based on the experimental and calculated results, the effect of temperature and alloying elements on corrosion rate and morphology was then extensively discussed.

2. Experimental Section

2.1. Materials

A Ni-based second-generation single crystalline superalloy SC2000 was used as the substrate in this study. It was aluminized by an industrially used chemical vapor deposition (CVD) method. The diffusion coating is with a thickness of around 60 μ m and can be divided into two parts with respect to the microstructure, as shown in **Figure 1**a. Referring to our previous study^[13] and Figure 1, the outer coating consisted of β -NiAl with a composition of around 50 at% Al, 5 at% Co, and 1 at% Cr and Cr-rich precipitates along the grain boundaries. The precipitate phases in the inner coating were identified as M_6C (M=W, Cr, Mo, Co) and μ phase A_6B_7 (A=Ni, Co and B=W, Mo), whereas the γ (Ni solid solution) and γ' (Ni₃Al) were identified as the substrate phases.

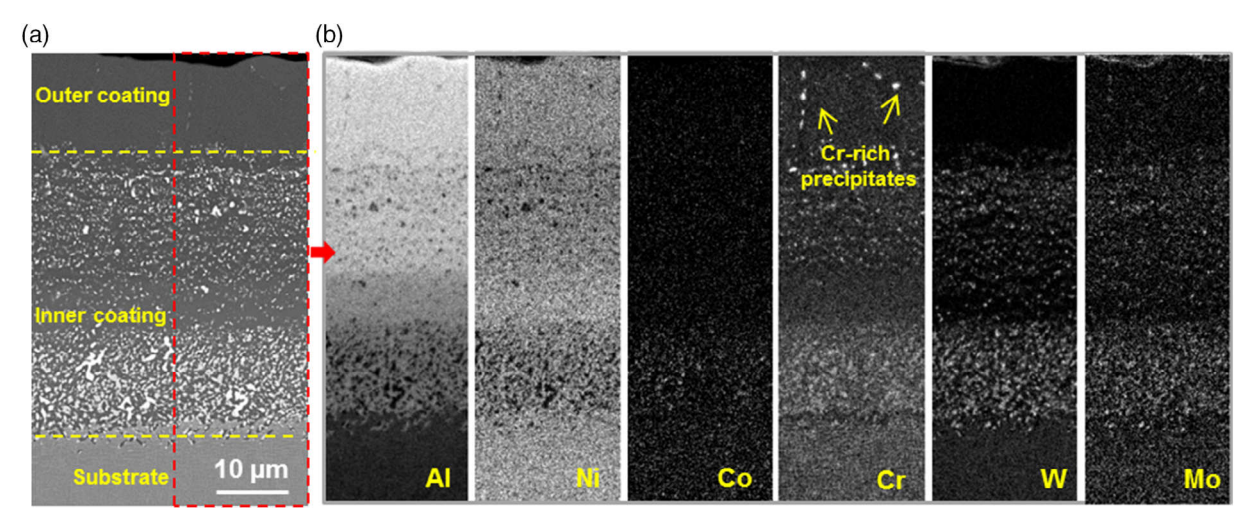


Figure 1. a) Back scatter electron (BSE) image and b) corresponding elements distribution maps obtained by energy-dispersive X-ray spectroscopy (EDS) of the cross section of the as-coated material.

www.aem-journal.com

ENGINEERING

www.advancedsciencenews.com

2.2. Experimental Procedure

Rectangular coupon specimens of $20 \times 10 \times 2 \text{ mm}^3$ were used for hot corrosion tests. 82 wt% dry salt powder was added into a special solvent, which consisted of 95 wt% terpineol and 5 wt% ethyl cellulose, to produce a deposit slurry. The dry salt mixture was 80 mol% Na₂SO₄-20 mol% K₂SO₄ (short for Na₂SO₄-20% K₂SO₄) and the melting temperature of this composition is 830 °C according to Na₂SO₄-K₂SO₄ phase diagram. [22] The binary salt mixture of Na2SO4 and K2SO4 is one of the standard mixtures used by the jet engine industry to evaluate the hot corrosion behavior of candidate materials for turbine blades. It was therefore chosen for this experimental program to evaluate the role of individual salt components in hot corrosion induced by complex deposits. This slurry was applied on one surface of the samples by painting, whereas an area of about $4 \times 10 \, \text{mm}^2$ at one sample end remained unpainted as a reference for the coating thickness loss measurements after corrosion tests. Prior to the hot corrosion tests, the painted samples were dried at 60 °C for 12 h. The final composition of the deposit after removing the solvent by drying was 99 wt% salt mixture + 1 wt% cellulose. Samples were weighed before painting and after drying. Around 30 mg cm⁻² salt mixture was applied onto the samples. The painted samples were then placed into alumina crucibles and exposed in a horizontally arranged furnace. A duplex reaction tube made of quartz (outer part) and sintered alumina (inner part) was used. The specimens were placed in the furnace at room temperature. The furnace was evacuated, filled with synthetic air-300 ppm SO₂, heated up to the specific temperature (600-800 °C), held for 24 h and cooled down to room temperature. Afterward, the furnace was filled with normal air and the specimens were taken out for subsequent investigation. Synthetic air-300 ppm SO₂ (SO₃ was produced by the reaction between O2 and SO2) gas flowed through a platinum honeycomb catalyst before flowing over the specimens to establish the equilibrium gas composition. The heating and cooling rate were 10 and 2 °C min⁻¹, respectively.

After exposure, all samples were mounted, ground, and polished to 0.25 µm surface finish using an oil-based solution to preserve any water-soluble species. The cross sections of the corroded samples were analyzed by scanning electron microscope (SEM) and energy dispersive X-ray spectroscopy (EDX) to characterize the distribution of main elements. The attack depth was determined by measuring the difference between the original

coating and the remaining coating thickness after exposure. As the initial coating thickness varied slightly from specimen to specimen, it was measured individually in the cross-section SEM images of the unpainted part. The remaining coating thickness was obtained by stitching multiple images with a length total of 10 mm in the cross section and measuring the distance between the attack front and the coating/substrate interface. As the attack front is irregular, 2000 values were gathered for each sample with a step of 5 µm in the sample surface direction. Maximum and mean values of the attack depth were calculated by comparing the coating thickness in the specimen part without deposit and remaining coating thickness affected by hot corrosion.

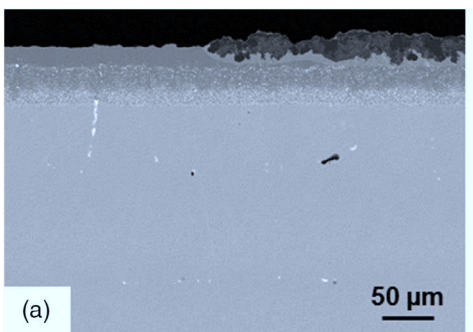
2.3. Thermodynamic Calculations

In this work, calculations were performed with software FactSage 7.2. [23,24] A thermodynamic database for sulfates system including Na_2SO_4 was in-house developed and was presented earlier. NiSO $_4$ was subsequently implemented into the database by modifying the description of solid and liquid solutions and adding Ni-containing compounds into it. The modification of the database is based on NiSO₄-Na₂SO₄ phase diagram and thermodynamic properties of relevant compounds. The extended database was used for the present calculation.

3. Experimental Results

3.1. Type II Hot Corrosion Morphology of β-NiAl Coating

The morphology of the specimen after exposure at 700 °C in air-300 ppm SO₂ for 24 h with Na₂SO₄-20% K₂SO₄ deposit is shown in Figure 2. A uniform corroded layer formed on the surface of the coating. Figure 2a shows both the specimen part covered by the salt mixture and the salt-free part. The salt-free part remained unattacked indicating that the β-NiAl phase was oxidation and sulfidation resistant in the current exposure condition, which is consistent with the literature. [28] To identify the corrosion products, EDX maps were obtained from the cross section, which are shown in Figure 3. A uniform aluminum-rich oxide layer penetrated by Na and K sulfates was observed as the main corrosion product (Figure 3d-h). It was found that Ni and Co not only dissolved into the sulfate, but also reprecipitated at the gas/scale interface as a thin oxide layer



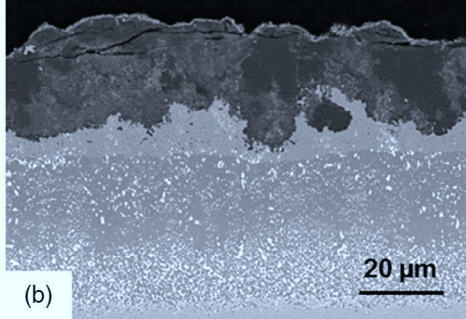


Figure 2. BSE images of the cross section of aluminized Ni-based superalloy after hot-corrosion testing at 700 °C in air-300 ppm SO₂ for 24 h: a) overview and b) hot corrosion morphology.

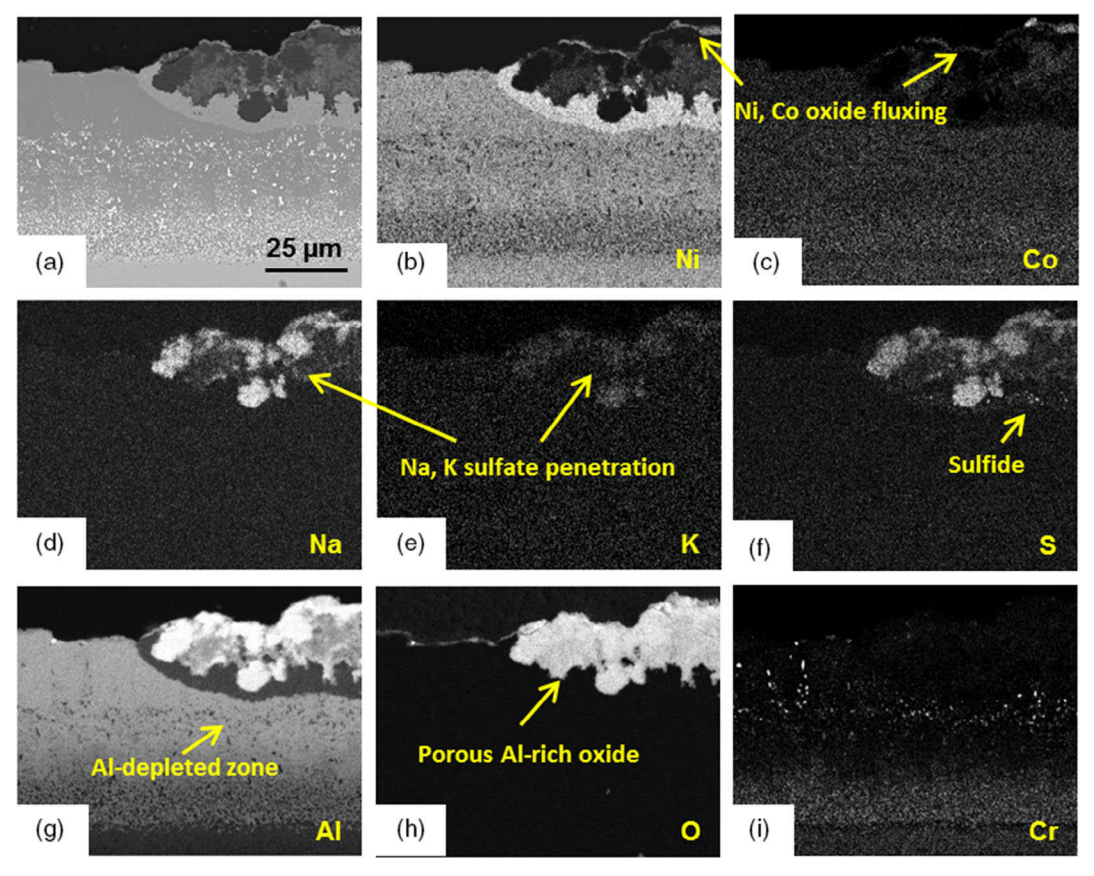


Figure 3. a) A SEM-BSE image and b-i) EDX-elemental maps of the cross section of the aluminized Ni-based superalloy after hot-corrosion testing at 700 $^{\circ}$ C air-300 ppm SO₂ for 24 h: corrosion products.

(Figure 3a,b). An Al-depleted zone was found to form beneath the scale (Figure 3g), which is attributed to the consumption of Al during the hot corrosion reaction. Moreover, sulfide particles were also observed in the Al-depleted zone (Figure 3f). To further identify the sulfide phase, EDX maps were performed at the Al-depleted zone. The maps in Figure 4 show that the particles are most likely Cr-rich sulfides.

3.2. Hot Corrosion Behavior of $\beta\textsc{-NiAl}$ Coating at Different Temperatures

Figure 5 and 6 shows the attack morphology and depth of type II hot corrosion of the β -NiAl coating induced by Na₂SO₄–20% K₂SO₄ in air-300 ppm SO₂ for 24 h at different temperatures.

The NiAl coating underwent negligible attack during exposure at $600\,^{\circ}\text{C}$ for 24 h, as shown in Figure 5a,b. Continuous Al-rich oxide layers were found both at 700 and 750 $^{\circ}\text{C}$ but no frontal attack was virtually observed at $800\,^{\circ}\text{C}$, as shown in Figure 5c–f. Both the mean value and the maximum value of the attack depth increased with increasing temperature and then dropped at $800\,^{\circ}\text{C}$, as shown in Figure 6. It demonstrates again that the studied kind of gas-induced acidic fluxing is very sensitive to exposure temperature.

Cr-rich precipitates were observed throughout the thickness of the as-received coating. As discussed in Section 2.1, this is typical for aluminide coatings, produced by high Al-activity CVD process. These precipitates are also found after the corrosion test at 800 °C in the inner part of the coating (**Figure 7**e). In the outer coating part, the preferential grain boundary attack occurred at

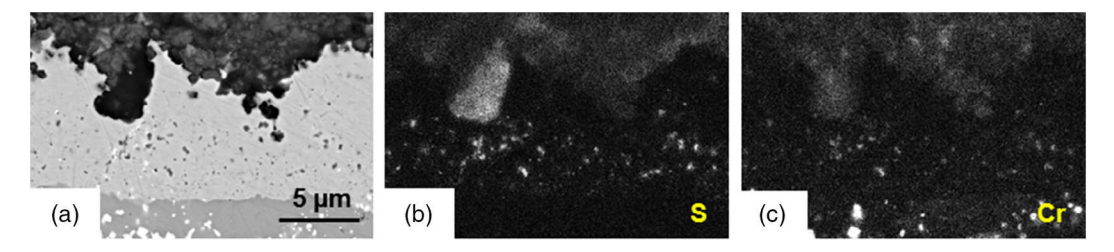


Figure 4. a) a SEM-BSE image and b,c) EDX-elemental maps of the cross section of the aluminized Ni-based superalloy in the Al-depleted zone after hot-corrosion testing at 700 $^{\circ}$ C air-300 ppm SO₂ for 24 h: chromium sulfide particles.



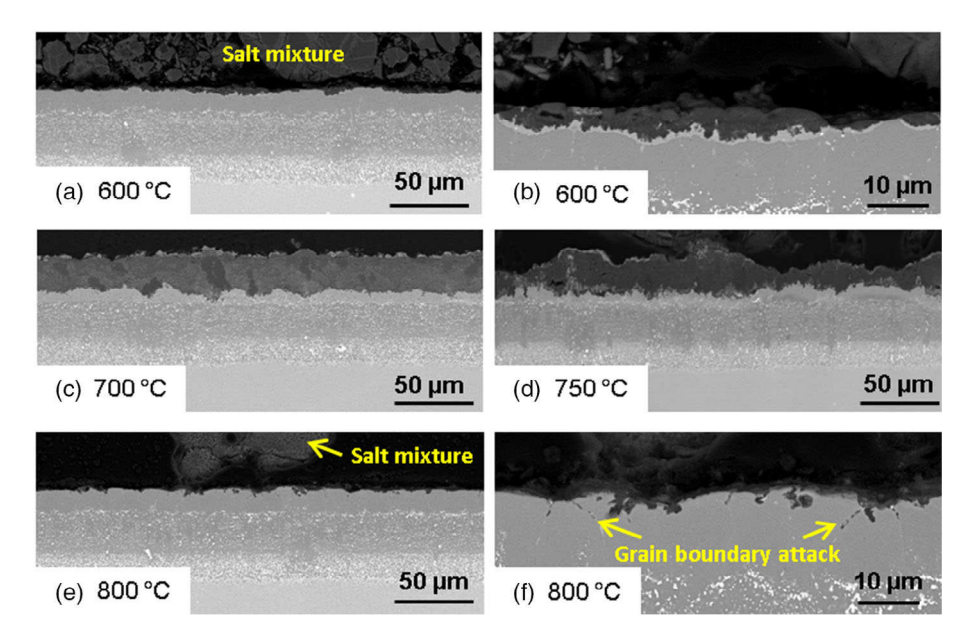


Figure 5. BSE cross-sectional image of studied aluminized Ni-based superalloy after hot-corrosion testing at a,b) 600 °C; c) 700 °C; d) 750 °C; and e,f) 800 °C in air-300 ppm SO₂ for 24 h.

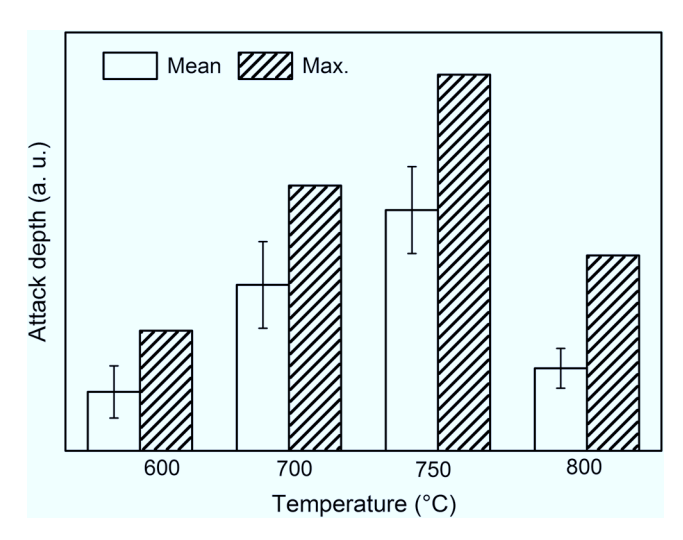


Figure 6. Attack depth of aluminized Ni-based superalloy after hotcorrosion testing at 600, 700, 750, and 800 °C in air-300 ppm SO₂ for 24 h.

800 °C after 24 h exposure, as shown in Figure 5e,f. The Cr-rich precipitates at grain boundaries, participated in corrosion reactions, which can be seen by comparing S, Na, Cr, and O maps along the corroded grain boundaries (Figure 7b,c,e,f). The initiation of grain boundary attack thus may result from the basic dissolution of transient Cr oxide into the sulfate. The detailed mechanism will be discussed in Section 5.2.

4. Thermodynamics of Na₂SO₄-NiO-SO₃ System

The experimental results indicate that the severest attack occurs at 700 and 750 °C, but not at 800 °C. To explain these observations, extensive thermodynamic assessment of the Na₂SO₄-NiO-SO₃ system was performed in this work.

4.1. Reactions for Liquid Formation in the Na2SO4-NiO-SO3 System

It is generally accepted that a liquid deposit is necessary to initiate severe type II hot corrosion^[2] although in some cases, considerable corrosion may result from solid deposits. [29] For Na₂SO₄-induced hot corrosion of Ni-based alloys (the effects of alloying elements are excluded in this section to simplify the reactions), the liquid phase forms via the reactions shown in Equation (1)–(4)

$$SO_2(g) + \frac{1}{2}O_2(g) = SO_3(g)$$
 (1)

$$NiO(s) + SO_3(g) = NiSO_4(s)$$
 (stoichiometric compound) (2)

 $NiSO_4(s) = NiSO_4(s.s)$ (dissolution into Na_2SO_4 solid solution) (3)

 $NiSO_4(s.s) = NiSO_4(l)$ (dissolution into Na_2SO_4 liquid solution)

$$\begin{aligned} &\text{NiO}\left(s\right) + \text{SO}_3(g) \\ &= \text{NiSO}_4(l) \\ &\text{(dissolution into Na}_2 \text{SO}_4 \\ &\text{liquid solution)} \end{aligned} \tag{5}$$

If the activity of NiO (s) is assumed to be 1, the Gibbs energy change of reaction (5) can be written as

$$\Delta G_{(5)}^{\circ} = -RT \ln \left(\frac{a_{\text{NiSO}_4}^L}{P_{\text{SO}_3}} \right) \tag{6}$$

www.advancedsciencenews.com

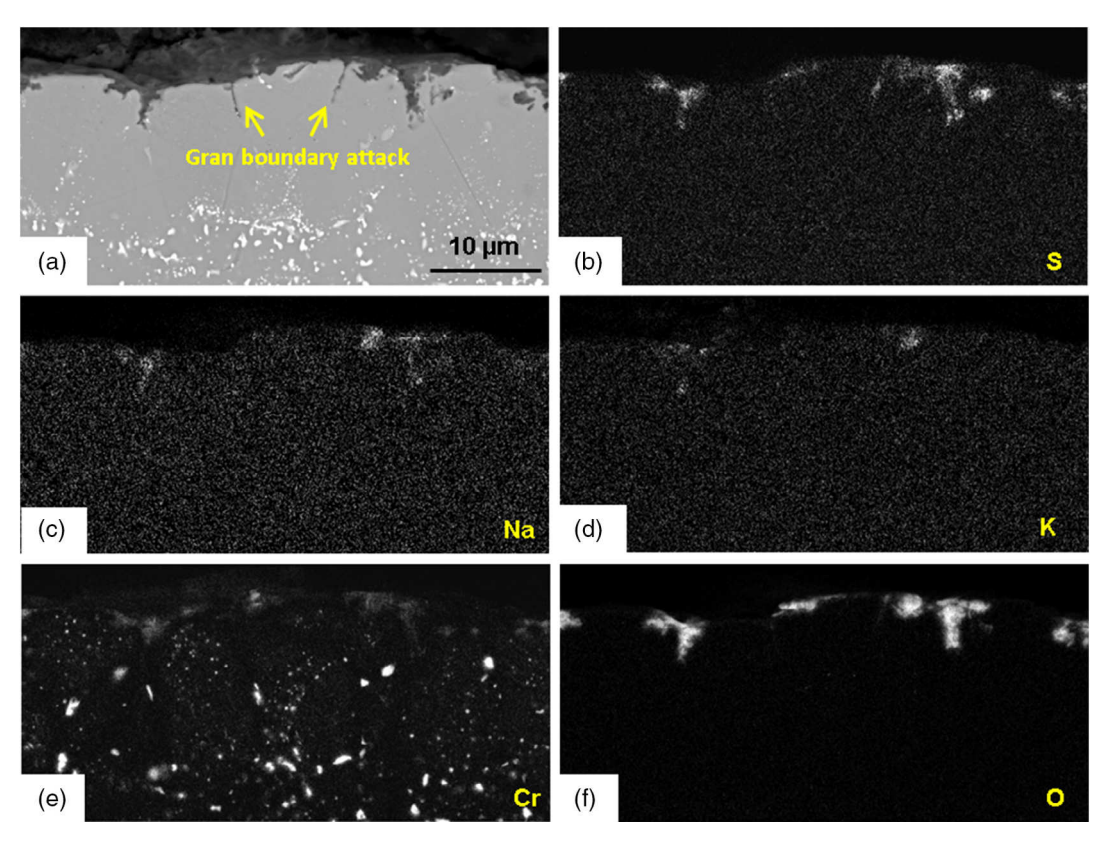


Figure 7. a) A SEM-BSE image and b-f) EDX-elemental maps of the cross section of the aluminized Ni-based superalloy after hot-corrosion testing at 800 °C in air-300 ppm SO₂ for 24 h.

where R is the gas constant and $a_{NiSO_4}^L$ is the activity of NiSO₄ in molten NiSO₄–Na₂SO₄ mixture.

The effect of temperature and SO_3 partial pressure on liquid formation can be estimated by Equation (6) based on the knowledge of the Gibbs energy change $(\Delta G_{(5)}^{\circ})$ and the activity of NiSO₄ in the molten salt $(a_{NiSO_4}^L)$.

4.2. Calculation of Na₂SO₄-NiO-SO₃ Stability Diagram

In this study, thermodynamic calculations were performed using the computational package FactSage. [23] An in-house-developed oxide database combined with the commercial database for pure substances SGPS^[30] was used for the equilibrium calculations under defined conditions. All available phase relations were considered by calculation: the Gibbs energy of a system is minimized to find the equilibrium state. The melting point of pure NiSO₄ and the entropy of melting were determined experimentally recently by Kobertz and Müller^[31] and included in the database. The stability phase diagram of Na2SO4-NiO-SO3 system as a function of temperature and SO₃ partial pressure was calculated by FactSage using the Phase diagram module. To represent the experimental conditions, O2, SO2/SO3, and inert gas (Ar) were chosen as gas constituents. The total gas pressure was set as 1 atm. The partial pressure of O2 was fixed at 0.21 atm, and the SO_3 partial pressure varied from 10^{-5} to 0.1 atm. About 0.62 $Na_2SO_4 + 0.38$ NiO was defined as the composition of the condensed phase, which is the eutectic composition of Na_2SO_4 –NiSO $_4$ system according to the binary phase diagram. [32] It should be noted that the results are obtained for equilibrium conditions only, and potential kinetic effects are not considered. Moreover, the calculation results should be validated for such complex system with respect to the reliability of implemented thermodynamic data mainly due to the assumptions made during the development of the thermodynamic database in view of the lack of experimental data.

The calculated stable phases are shown as a function of temperature and SO₃ partial pressure in Figure 8a (solid blue curves). It shows that only solid phases are stable, when the temperature is lower than the eutectic of NiSO₄ and Na₂SO₄, namely $671\,^{\circ}\text{C}$. In the temperature range between NiSO₄– Na_2SO_4 eutectic and the melting point of Na_2SO_4 , as p_{SO_3} increases to a certain level, the stable liquid starts to form. To compare the experimental data to the calculation results, SO3 partial pressure for air-300 ppm SO₂ as a function of temperature was also calculated by FactSage Equilibrum module and superimposed on the data in Figure 8a,b (green dashed lines). The minimum p_{SO} , required for liquid formation (bottom blue line in Figure 8a) increases with increasing temperature; however, the equilibrium constant of reaction (1) for SO₃ production from SO₂ decreases at the same time (green dashed line in Figure 8a,b) as is well known from literature. [8] It is therefore inferred that the formation of NiSO₄-Na₂SO₄ liquid is suppressed at the higher temperatures (but below the melting temperature of the deposit) in a given atmosphere with a fixed ratio of oxygen to

ENGINEERING

www.advancedsciencenews.com

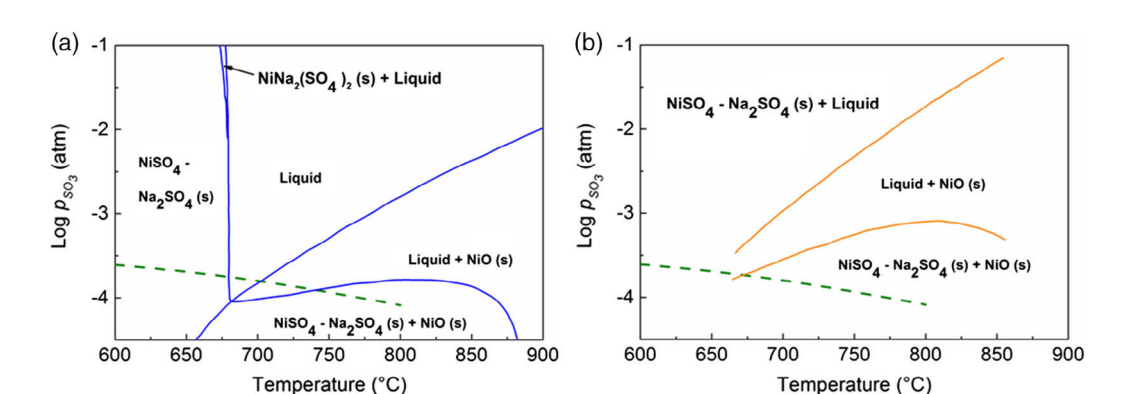


Figure 8. Stability diagrams of Na₂SO₄–NiO–SO₃ system superimposed with p_{SO_3} as a function of temperature in fixed $p_{O_2} = 0.21$ and $p_{SO_2/SO_3} = 300$ ppm atm. (green dashed curve): a) calculated using an in-house-developed database by FactSage (blue solid curves); b) Calculated by Misra et al.^[11] (orange solid curves).

sulfur. Occurrence of the attack at 800 °C is therefore not favored according to the stability calculation.

4.3. Comparison of the Stability Diagram to that Calculated from the Literature

The stability diagram calculated by Misra et al.^[11] is also shown in Figure 8b (orange solid curves) for comparison. It is found that the minimum p_{SO_2} for liquid stabilization predicted by the present calculation (bottom blue line in Figure 8a) is substantially lower than that calculated by Misra (bottom orange line in Figure 8b). Such discrepancy can be attributed to the following reasons: 1) The activity of NiSO₄ in the liquid solution was estimated in Misra's work using a regular solution model with an interaction energy parameter $\omega_{\rm L}$, which was assumed to be independent of temperature and composition. However, below 827 °C, using $\omega_{\rm L}$ may not be a good approximation, because at lower temperatures, the concentration of NiSO₄ in the liquid is relatively high, and the solution cannot be regarded as a dilute solution. In this work, the interaction between NiSO4 and Na₂SO₄ in the liquid was calculated considering the effect of temperature and composition for all temperatures; 2) In Misra's study, the standard Gibbs free energy change of reaction (5) at lower temperatures was obtained by the extrapolation of the high-temperature (827-900 °C) values, apparently associated with significant errors. The melting point and the enthalpy of NiSO₄ fusion estimated by Misra based on his proposed model were 1306 K and 32.8 kJ·mol⁻¹ (7.84 kcal·mol⁻¹), respectively, which are substantially lower than the values recently reported by Kobertz and Müller^[31] based on more accurate measurements $(1483 \pm 3 \text{ K and } 44 \pm 2 \text{ kJ} \cdot \text{mol}^{-1}, \text{ respectively}).$

5. Discussion

Type II hot corrosion behavior of coated commercial Ni-based superalloys under mixed sulfate deposits is very complex, not only because of complex reactions between Ni, salts and the gas, but also due to the fact that different alloying elements and salt components may get involved into the reactions. In addition, the main reactions between the alloy and salts

are very sensitive to the gas composition and the exposure temperature.

5.1. Comparison between Corrosion Experiments and Thermodynamic Predictions

To simplify the system and better understand the mechanisms, the effect of temperature on the reactions between Ni, Na₂SO₄, O2, and SO2/SO3 was studied from the thermodynamic point of view in this study. As shown in Figure 8a (the bottom blue curve), the minimum SO₃ partial pressure required to stabilize the Na₂SO₄-NiSO₄ liquid solution increases with increasing temperature between \approx 670 and 820 °C. At the same time, p_{SO_3} in the studied air-SO₂/SO₃ atmosphere decreases with increasing temperature (Figure 8a,b). Therefore, the overall tendency to form Na₂SO₄-NiSO₄ liquid decreases with increasing temperature in the investigated temperature range. According to our thermodynamic calculation (Figure 8a), Na₂SO₄-NiSO₄ liquid is expected to be stabilized by 300 ppm SO₂ at 700 °C but not at 800 °C. In these experiments, a pronounced frontal attack was observed at 700 °C but not found at 800 °C after 24 h exposure (Figure 5c,e,f), which is in excellent agreement with the calculations in Figure 8a. It can be concluded that the initiation of the attack is strongly governed by the NiSO₄-Na₂SO₄ liquid stability and therefore by the gas composition and the exposure temperature, even for such a complex coated material. At 750 °C, pronounced attack was observed, as shown in Figure 5d; however, the calculated SO₃ partial pressure in the atmosphere is slightly below that necessary to stabilize the liquid phase. The reasons for the variation between the experimental and calculation results at 750 °C will be discussed in Section 5.2.

5.2. Possible Mechanisms of Hot Corrosion Reactions at Different Temperatures

5.2.1. 600°C

Although $600\,^{\circ}\text{C}$ is below the eutectic temperature of NiSO₄–Na₂SO₄, a minor corrosion attack was found after 24 h exposure

ENGINEERING

www.advancedsciencenews.com www.aem-journal.com

(Figure 5a,b). Cobalt oxide was found in the corroded layer at the gas/deposit interface after exposure at 600 °C (not shown here), as well as at 700 °C (Figure 3c). The eutectic temperature of $\text{Na}_2\text{SO}_4\text{--CoSO}_4$ and $\text{K}_2\text{SO}_4\text{--CoSO}_4$ are 565 $^{\circ}\text{C}^{[8]}$ and 540 $^{\circ}\text{C},^{[33]}$ respectively. Thus, the attack at 600 °C may result from the presence of Co in the coating and Na₂SO₄/K₂SO₄-CoSO₄ liquid formation. In addition, Kistler et al. [29] recently proposed a new solid-state model for hot corrosion at temperatures below 700 °C. They found a metastable-phase Na₂NiSO₅ at the interface between Na2SO4 and NiO and at the grain boundaries of the Na₂SO₄ deposit, which provided short-circuit paths for Ni outward diffusion, thereby accelerating the corrosion process. According to their study, a similar compound was also found when K₂SO₄ was used as the deposit. Such solid-state reaction and diffusion of Ni could also explain the minor hot corrosion attack observed at 600 °C in this study.

5.2.2. 700°C

In this study, NiO was found on the surface of the corroded layer (Figure 3b), which demonstrated the outward diffusion of nickel ions in the molten salt and the reprecipitation of NiO on the very surface. A similar phenomenon was also observed in several Ni-based alloys by other researchers. [16,20,34] However, in pure nickel case, the dissolution of NiO into the salt was found to stop once the melt was saturated, thereby hindering NiO reprecipitation on the surface of the salt.^[19] As the solubility of NiO displayed a positive gradient toward the gas/salt interface, there was apparently no driving force for outward diffusion of Ni ions. But the acidity of the melt and the solubility of NiO in it can be substantially modified by addition of alloying elements. This effect was attributed to the synergistic dissolution of various oxides, e.g., NiO, Co₂O₃, Al₂O₃, and Cr₂O₃. [16,35] For hot corrosion of a commercial alloy or a complex coating, at the salt/oxide interface, as SO₃ was consumed by oxidation and sulfidation during exposure, the basicity of the salt was claimed to increase locally, which allowed the basic fluxing of Al₂O₃ and Cr₂O₃, and released SO3. The localized acidity of the salt will thus in turn be increased, resulting in the increase in the solubility of NiO and Co₂O₃ in the salt. Therefore, with the assistance of Al₂O₃ and Cr₂O₃, continuous NiO dissolution, transport to the surface, and reprecipitation can occur. Al₂O₃ and Cr₂O₃ will most likely precipitate locally at the sites where the basic fluxing is no longer satisfied, as demonstrated in this study by the porous Al-rich oxide layer in Figure 3g.

5.2.3. 750°C

Severe uniform attack was found at 750 °C after 24 h exposure (Figure 5d), whereas stable Na₂SO₄–NiSO₄ can barely form under the exposure condition according to the thermodynamic calculation. One possible reason for this discrepancy is the presence of various alloying elements in the coating. Co oxide is found on the surface of and within the corrosion products after exposure at 700 °C (Figure 3) and 750 °C (not shown here). Na₂SO₄–CoSO₄ and K₂SO₄–CoSO₄ liquid may form at 750 °C in the presence of lower SO₃ partial pressure. In addition, the synergistic oxides' dissolution mechanism, as is discussed for

700 °C may also applicable for 750 °C. Finally, the addition of K_2SO_4 into the deposit may also alter the minimum p_{SO_3} required for NiSO₄–Na₂SO₄ liquid formation by other reactions. A thermodynamic verification of the influence of K_2SO_4 addition is not possible now due to the absence of thermodynamic data.

5.2.4. 800°C

After 24 h exposure at 800 °C, no frontal attack was found. The main reason is likely to be that no stable NiSO₄-Na₂SO₄ liquid can form at 800 °C in the present experimental condition. In addition, the tendency of protective alumina formation increase at 800 °C compared with lower temperatures. Nevertheless, preferential grain boundary attack was found at 800 °C (Figure 7). Apart from Ni and Co, other alloying elements may also form liquid phases together with the deposits and cause basic fluxing when the basicity of the salt allows. One particular important element in this study is Cr. Referring to the Na₂SO₄-Na₂CrO₄-K₂SO₄-K₂CrO₄ phase diagram, [36] the minimum melting temperature of this system is 752 °C, and the melting point of Na₂CrO₄ is 792 °C. It is therefore inferred that the grain boundary attack may be attributed to the oxidation of Cr-rich precipitates followed by the basic dissolution of Cr₂O₃ into the Na₂SO₄-K₂SO₄ solid solution resulting in the local salt melting. Further studies are necessary to verify this assumption.

6. Conclusions

Na₂SO₄-20% K₂SO₄ slurry was applied on the surface of an aluminized second-generation single crystalline Ni-based superalloy and then the samples were exposed to 600-800 °C with air-300 ppm SO₂. Phase stabilities were calculated in the system Na-Ni-S-O by FactSage using an in-house-developed database. Based on the experimental and calculation results, following conclusions can be drawn: 1) The reaction morphologies between 600 and 750 °C are similar. The primary and main characteristics are the formation of a thick aluminum-rich porous oxide layer with Ni- and Co-rich oxides above Na and K sulfates penetration inside, Al-depleted layer containing sulfide particles underneath it; 2) Much more severe attack occurred at 700 °C compared with those at 600 and 800 °C after 24 h exposure, indicating that the corrosion rate is strongly governed by Na₂SO₄-NiSO₄ liquid formation. The test temperature affects the attack rate of the outer coating (mainly β-NiAl phase) by changing the minimum p_{SO_3} necessary to stabilize this liquid; 3) The experimental observations at 600, 700, and 800 °C correspond well with the thermodynamic calculations. At 750 °C, high corrosion rate was observed contrary to the thermodynamic predictions showing no liquid phases forming in the prevailing SO₃ content. This might be related to the effect of K₂SO₄ or that of alloying elements such as Co and Cr in the coating; 4) No frontal attack was observed after 24 h corrosion testing at 800 °C most likely because the Na₂SO₄-NiSO₄ liquid is unstable at the test condition. However, at the coating grain boundary, a local attack was identified. The enrichment of Cr at grain boundaries might promote the attack by reacting with the deposit; 5) The stability diagram of Na₂SO₄-NiO-SO₃ was calculated by FactSage using an in-house-developed database. The trend of calculated p_{SO_2} and



www.advancedsciencenews.com

www.aem-journal.com

ENGINEERING

well [11] A. K. Misra, D. P. Whittle, W. L. Worrell, *J. Electrochem. Soc.* **1982**, the 129, 1840. [12] J. R. Nicholls, *JOM* **2000**, *52*, 28. [13] R. Pillai, A. Chyrkin, D. Grüner, W. Nowak, N. Zheng, A. Kliewe,

temperature dependence for liquid formation corresponds well with the literature but the minimum $p_{\rm SO_3}$ for stabilizing the liquid phase predicted by the present calculation is substantially lower than that estimated in the previous studies. Due to an improved liquid solution model and updated thermodynamic properties, the current calculation showed a better quantitative correlation with the experimental observations.

Acknowledgements

Mr. H. Cosler is kindly acknowledged for performing the hot corrosion tests. The authors are grateful to Dr. E. Wessel and Dr. D. Grüner for the SEM analysis. The authors are grateful to China Scholarship Council (no. 201708440229) for the financial support of this work. This work has also been supported by the German Federal Ministry of Economics under grant nos. 20T1522A and 0327773K and MTU Aero Engines AG.

Conflict of Interest

The authors declare no conflict of interest.

Keywords

aluminide coatings, Na_2SO_4 – K_2SO_4 deposits, temperature dependence, type II hot corrosion

Received: October 15, 2019 Revised: January 1, 2020 Published online: February 21, 2020

- [1] N. S. Bornstein, JOM 1996, 48, 37.
- [2] N. Birks, G. H. Meier, F. S. Pettit, Introduction to the High-Temperature Oxidation of Metals, Cambridge University Press, Cambridge 2006, pp. 206–252.
- [3] F. Pettit, Oxid. Met. 2011, 76, 1.
- [4] K. L. Luthra, Metall. Trans. A 1982, 13A, 1853.
- [5] A. K. Misra, D. P. Whittle, Oxid. Met. 1984, 22, 1.
- [6] J. A. Goebel, F. S. Pettit, G. W. Goward, Metall. Trans. 1973, 4, 261.
- [7] L. Shi, Y. Zhang, S. Shih, Oxid. Met. 1992, 38, 385.
- [8] D. A. S. K. L. Luthra, J. Electrochem. Soc. 1980, 127, 2202.
- [9] K. L. Luthra, Metall. Trans. A 1982, 13A, 1843.
- [10] A. K. Misra, D. P. Whittle, W. L. Worrell, J. Electrochem. Soc. 1980.

- W. J. Quadakkers, Surf. Coat. Technol. 2016, 288, 15. [14] T. Gheno, M. Zahiri Azar, A. H. Heuer, B. Gleeson, Corros. Sci. 2015,
- [14] T. Gheno, M. Zahiri Azar, A. H. Heuer, B. Gleeson, Corros. Sci. 2015, 101, 32.
- [15] B. S. Lutz, J. M. Alvarado-Orozco, L. Garcia-Fresnillo, G. H. Meier, Oxid. Met. 2017, 88, 599.
- [16] J. M. Alvarado-Orozco, J. E. Garcia-Herrera, B. Gleeson, F. S. Pettit, G. H. Meier, Oxid. Met. 2018, 90, 527.
- [17] J. A. Goebel, F. S. Pettit, Metall. Trans. 1970, 1, 3421.
- [18] W.-J. Zhang, R. Sharghi-Moshtaghin, Metall. Mater. Trans. A 2018, 49, 4362.
- [19] T. Gheno, B. Gleeson, Oxid. Met. 2015, 84, 567.
- [20] M. N. Task, B. Gleeson, F. S. Pettit, G. H. Meier, Oxid. Met. 2013, 80, 125.
- [21] R. L. Jones, S. T. Gadomski, J. Electrochem. Soc. 1982, 129, 1613.
- [22] H. Du, J. Phase Equilib. 2000, 21, 6.
- [23] C. W. Bale, E. Bélisle, P. Chartrand, S. A. Decterov, G. Eriksson, A. E. Gheribi, K. Hack, I. H. Jung, Y. B. Kang, J. Melançon, A. D. Pelton, S. Petersen, C. Robelin, J. Sangster, P. Spencer, M. A. Van Ende, Calphad 2016, 54, 35.
- [24] FactSage (Facility for the Analysis of Chemichal Thermodynamics), Version 7.2, CRCT-ThermFact Inc. (Montreal) and GTT-Technologies, (Germany), 1976-2019.
- [25] K. Hack, T. Jantzen, M. Müller, E. Yazhenskikh, G. Wu, in 5th Int. Congress on the Science and Technology of Steelmaking, Dresden, Germany 2012.
- [26] E. Yazhenskikh, T. Jantzen, K. Hack, M. Muller, *PACПЛАВЫ* **2019**, 2, 116.
- [27] E. Yazhenskikh, K. Hack, T. Jantzen, D. Kobertz, M. Müller, in CALPHAD XLIV, Loano, Italy 2015.
- [28] H. J. Grabke, M. W. Brumm, B. Wagemann, *Mater. Corros.* 1996, 47, 675.
- [29] E. Kistler, W.-T. Chen, G. H. Meier, B. Gleeson, *Mater. Corros.* 2019, 70, 1346
- [30] SGPS-SGTE Pure Substances database (v13.1), 2017, http://www.factsage.com/facthelp/FSNew_Databases.htm#SGPS.
- [31] D. Kobertz, M. Müller, Calphad 2014, 45, 55.
- [32] K. A. Bol'shakov, P. I. Fedorov, Zhur. Obshchei Khimii 1956, 26.
- [33] G. Calcagni, D. Marotta, Gazz. Chim. Ital. 1914, 43, 380.
- [34] J. Sumner, A. Encinas-Oropesa, N. J. Simms, J. R. Nicholls, Oxid. Met. 2013, 80, 553.
- [35] Y.-S. Hwang, R. A. Rapp, J. Electrochem. Soc. 1990, 137, 1276.
- [36] W. W. Liang, P. L. Lin, A. D. Pelton, High Temp. Sci. 1980, 12, 71.